Density Functional Calculations of Electronic *g*-Tensors Using Spin−Orbit Pseudopotentials and Mean-Field All-Electron Spin−Orbit Operators

Olga L. Malkina,[†,‡] Juha Vaara,[§] Bernd Schimmelpfennig,[∥] Markéta Munzarová,[⊥] Vladimir G. Malkin,*[,‡] and Martin Kaupp*[,#]

Contribution from the Computing Center and Institute of Inorganic Chemistry, Slovak Academy of Sciences, Dubravska Cesta 9, SK-84236 Bratislava, Slovakia, Max-Planck-Institut für Festkörperforschung, Heisenbergstrasse 1, D-70569 Stuttgart, Germany, Institut für Anorganische Chemie, Universität Würzburg, Am Hubland, D-97074 Würzburg, Germany

Received March 20, 2000. Revised Manuscript Received June 29, 2000

Abstract: Modern density-functional methods for the calculation of electronic *g*-tensors have been implemented within the framework of the deMon code. All relevant perturbation operators are included. Particular emphasis has been placed on accurate yet efficient treatment of the two-electron spin−orbit terms. At an all-electron level, the computationally inexpensive atomic mean-field approximation is shown to provide spin−orbit contributions in excellent agreement with the results obtained using explicit one- and two-electron spin−orbit integrals. Spin−other−orbit contributions account for up to 25−30% of the two-electron terms and may thus be non-negligible. For systems containing heavy atoms we use a pseudopotential treatment, where quasirelativistic pseudopotentials are included in the Kohn−Sham calculation whereas appropriate spin−orbit pseudopotentials are used in the perturbational treatment of the *g*-tensors. This approach is shown to provide results in good agreement with the all-electron treatment, at moderate computational cost. Due to the atomic nature of both mean-field all-electron and pseudopotential spin−orbit operators used, the two approaches may even be combined in one calculation. The atomic character of the spin−orbit operators may also be used to analyze the contributions of certain atoms to the paramagnetic terms of the *g*-tensors. The new methods have been applied to a wide variety of species, including small main group systems, aromatic radicals, as well as transition metal complexes.

1. Introduction

Electron paramagnetic resonance (EPR) spectroscopy is one of the most important experimental techniques of studying compounds containing unpaired electrons. Typical applications encompass biological systems, paramagnetic defects in extended solids, transition metal complexes, or simple organic radicals (e.g., in zeolites). The recent development of high-field EPR spectroscopy (at frequencies of 95 GHz or higher) has significantly widened the scope of the method and of the information that may be extracted. In particular, in modern solid-state EPR experiments the components of the electronic *g*-tensor may frequently be resolved.[1] Interpretation of these experiments by quantum chemical calculations has thus become highly desirable. However, in contrast to the treatment of EPR hyperfine coupling constants that already do have an appreciable history of first principles theoretical treatments,[2] quantitative calculations of electronic *g*-tensors by the machinery of nonempirical quantum chemistry have become possible only very recently (for semiempirical calculations, cf. refs 3 and 4; see also ref 5).

The first accurate calculations at the Hartree−Fock (HF) and multireference configuration interaction (MRCI) levels of theory are due to Lushington et al.[6,7] Vahtras and co-workers[8] have employed HF and multiconfiguration self-consistent-field (MCSCF) linear response functions. These ab initio implemen-

[†] Computing Center, Slovak Academy of Sciences.

[‡] Institute of Inorganic Chemistry, Slovak Academy of Sciences, E-mail: malkin@savba.sk.

[§] Max-Planck-Institut für Festkörperforschung. Present address: Department of Chemistry, P.O. Box 55 (A.I. Virtasen aukio 1), FIN-00014 University of Helsinki, Finland.

[∥] Max-Planck-Institut für Festkörperforschung. Present address: Theoretical Chemistry, Teknikringen 30, Royal Institute of Technology, S-10044 Stockholm, Sweden.

[⊥] Max-Planck-Institut für Festkörperforschung. Present address: Department of Theoretical and Physical Chemistry, Faculty of Science, Masaryk University, Kotlárská 2, CZ-61137 Brno, Czech Republic.

[#] Institut für Anorganische Chemie, Universität Würzburg. Telephone: +49−931-888-5281. Fax: +49−931-888-7135. E-mail: kaupp@mail.uni-wuerzburg.de.

(1) See, for example: (a) Möbius, K. In *Biological Magnetic Resonance*; Berliner, L. J., Reuben, J., Eds.; Plenum Press: New York, 1993; Vol. 13, pp 253−274. (b) Prisner, T. F. In *Advances in Magnetic and Optical Resonance*; Warren, W., Ed.; Academic Press: New York, 1997; Vol. 20, pp 245−299.

(2) Engels, B.; Eriksson, L. A.; Lunell, S. *Adv. Quantum Chem.* **1996**, *27*, 297.

(3) See, for example: Angstl, R. *Chem. Phys.* **1989**, *132*, 435. Plakhutin, B. N.; Zhidomirov, G. M.; Zamaraev, K. I. *J. Struct. Chem.* **1983**, *24*, 3.

(4) See, for example: Un, S.; Atta, M.; Fontcave, M.; Rutherford, A. W. *J. Am. Chem. Soc.* **1995**, *117*, 10713.

(5) For DFT calculations of *g*-tensors with semiempirical SO operators cf., for example: Geurts, P. J. M.; Bouten, P. C. P.; van der Avoird, A. J. *Chem. Phys.* **1980**, *73*, 1306. Belanzoni, P.; Baerends, E. J.; van Asselt, S.; Langewen, P. B. *J. Phys. Chem.* **1995**, *99*, 13094. Swann, J.; Westmoreland, T. D. *Inorg. Chem.* **1997**, *36*, 5348.

(6) Lushington, G. H.; Grein, F. *Theor. Chim. Acta* **1996**, *93*, 259. Bruna, P.; Lushington, G. H.; Grein, F. *Chem. Phys.* **1997**, *225*, 1.

(7) Lushington, G. H. Ph.D. Thesis, The University of New Brunswick, Canada, 1996.

(8) Engström, M.; Minaev, B.; Vahtras, O.; Ågren, H. *Chem. Phys.* **1998**, *237*, 149. Vahtras, O.; Minaev, B.; Ågren, H. *Chem. Phys. Lett.* **1997**, *281*, 186.

10.1021/ja000984s CCC: $19.00
Published on Web 09/13/2000

tations include essentially all perturbation operators—at the Breit−Pauli level of treating spin−orbit coupling—which are thought to be relevant for the electronic *g*-tensor. Thus, at least for systems containing only light elements, it is in principle possible to converge to the experimental results, by using larger and larger basis sets and by improving the treatment of electron correlation. However, obviously such calculations are at present largely restricted to relatively small systems, as the accurate inclusion of electron correlation becomes very demanding with increasing size of the system.

In case of the NMR nuclear shielding tensor, which is conceptually related to the electronic *g*-tensor, it has recently been shown that density-functional theory (DFT) provides a valuable alternative to post-HF treatment, by approximately including electron correlation at lower computational cost.[9−11] Indeed, a recent state-of-the-art DFT implementation of *g*-tensor calculations, reported by Schreckenbach and Ziegler (SZ),[12] was based on their previous NMR chemical shift implementation (using gauge-including atomic orbitals, GIAOs) in the Amsterdam density-functional (ADF) program. A different DFT-GIAO implementation (but also in the ADF code), using the two-component zero-order regular approximation (ZORA[13]) to account for spin−orbit (SO) coupling and scalar relativity, has been reported by van Lenthe et al.[14] A two-component UHF approach has been implemented by Jayatilaka.[15]

Here we report an alternative DFT implementation of electronic *g*-tensors within the deMon[16,17] code. Our method differs from SZ mainly in the way we deal with spin−orbit coupling. SZ used an effective Kohn−Sham potential to model approximately the two-electron SO terms.[12] This treatment does not include the spin−other−orbit terms, and it also involves a number of other approximations. We have recently shown for calculations of SO corrections to NMR chemical shifts that (1) a mean-field one-center approximation to the full two-electron SO integrals gives results in excellent agreement with an exact treatment, at a small fraction of the computational effort;[18] (2) spin−orbit pseudopotentials (spin−orbit effective-core potentials, SO-ECPs) do also provide a good approximation to the full SO operator, in a valence-only treatment, and they allow easily the simultaneous treatment of SO and scalar relativistic effects.[19] Our new *g*-tensor code is based on these efficient and accurate "atomic" treatments of SO coupling. This leads to a number of advantages in the calculations, as well as in the subsequent interpretation of the results, as we will demonstrate.

2. Methods

We define the *g*-tensor as

$$\mathbf{g} = g_e\mathbf{1} + \Delta\mathbf{g} \tag{1}$$

and focus on *g*-shifts (Δg components) relative to the free electron *g*-value. Throughout this work, *g*-shifts are given in ppm for main group radicals and in ppt (parts-per-thousand) for most transition metal systems (more significant digits are typically not available from experiment anyway).

The second-order theory for calculating $\Delta\mathbf{g}$ within a one-component approach has been presented in several recent reports of modern quantum chemical implementations.[6−8,12,20] Hence, we limit ourselves to recapitulating only the relevant points and give the final expressions used in our present DFT calculations. Here we investigate radicals with doublet electronic ground states only. We look for terms bilinear in the magnetic field $\mathbf{B}_0$ and effective electronic spin $\mathbf{s}$ in the molecular energy expression E; hence, the Cartesian $u\upsilon$-component of $\Delta\mathbf{g}$ is

$$\Delta g_{u\upsilon} = \frac{1}{\mu_B}\frac{\partial^2 E}{\partial B_{0,u}\partial s_\upsilon}\bigg|_{\mathbf{B}=\mathbf{s}=0} \tag{2}$$

We shall employ atomic units based on the SI system, where the Bohr magneton $\mu_B = {}^1/_2$.

The main contributions to the $\Delta\mathbf{g}$ tensor up to $O(\alpha^2)$ (α is the fine-structure constant) arise from the SO coupling Hamiltonian

$$H_{SO} = \frac{\alpha^2}{4}g_e\left[\sum_M Z_M \sum_i \frac{\mathbf{s}_i\cdot\mathbf{l}_{iM}}{r_{iM}^3} - \sum_{ij}{}' \frac{(\mathbf{s}_i + 2\mathbf{s}_j)\cdot\mathbf{l}_{ij}}{r_{ij}^3}\right] \tag{3}$$

where $Z_M e$ is the charge of nucleus M, $\mathbf{s}_i$ the spin of electron i, $\mathbf{l}_{iM} = (\mathbf{r}_i - \mathbf{R}_M) \times [-i\nabla_i + \mathbf{A}_0(\mathbf{r}_i)]$ the angular momentum of electron i with respect to the position of nucleus $M(\mathbf{R}_M)$, and $\mathbf{l}_{ij} = (\mathbf{r}_i - \mathbf{r}_j) \times [-i\nabla_i + \mathbf{A}_0(\mathbf{r}_i)]$ the corresponding angular momentum with respect to the position of electron $j(\mathbf{r}_j)$. Here, $\mathbf{A}_0(\mathbf{r}_i) = {}^1/_2\mathbf{B}_0 \times (\mathbf{r}_i - \mathbf{O})$ is the vector potential at $\mathbf{r}_i$ corresponding to the external magnetic field. We note that at the present level of accuracy of both the theory and experiment, it is not necessary to distinguish between g_e and the *g*-factor associated with the SO interaction.[20,21] The field-independent part of H_{SO} (arising from the $-i\nabla_i$ terms in eq 3) couples, in double perturbation theory, with the orbital Zeeman (OZ) interaction

$$H_{OZ} = \frac{1}{2}\sum_i \mathbf{l}_{iO}\cdot\mathbf{B}_0 \tag{4}$$

to the sum-over-states density-functional perturbation theory (SOS-DFPT)[22] expression for the paramagnetic part of $\Delta\mathbf{g}$

$$\Delta g_{SO/OZ,u\upsilon} = \frac{\alpha^2}{2}g_e\left[\sum_k^{occ(\alpha)}\sum_a^{virt(\alpha)}\frac{\langle\psi_k^\alpha|H_{SO,\upsilon}|\psi_a^\alpha\rangle\langle\psi_a^\alpha|l_{O,u}|\psi_k^\alpha\rangle}{\epsilon_k^\alpha - \epsilon_a^\alpha - \Delta E_{k\to a}^{xc}} - \sum_k^{occ(\beta)}\sum_a^{virt(\beta)}\frac{\langle\psi_k^\beta|H_{SO,\upsilon}|\psi_a^\beta\rangle\langle\psi_a^\beta|l_{O,u}|\psi_k^\beta\rangle}{\epsilon_k^\beta - \epsilon_a^\beta - \Delta E_{k\to a}^{xc}}\right] \tag{5}$$

Here, $\psi_k^{\alpha/\beta}$ and $\psi_a^{\alpha/\beta}$ are unperturbed occupied and virtual α/β MOs, respectively. ϵ_k and ϵ_a are the corresponding Kohn−Sham eigenvalues, and $\Delta E_{k\to a}^{xc}$ is the "SOS-DFPT correction" (Loc.1 in the present paper) imposed on the energy denominators.[17,22] We refer to the original papers for details. Leaving the $\Delta E_{k\to a}^{xc}$ term out corresponds to the uncoupled DFT (UDFT) approximation. $H_{SO,\upsilon}$ denotes the υ-component of the spatial part of the field-free SO Hamiltonian (the prefactors $\alpha^2\, g_e/4$ of H_{SO} of eq 3 have been absorbed in the prefactor of eq 5). While the

(9) Kaupp, M.; Malkina, O. L.; Malkin, V. G. In *Encyclopedia of Computational Chemistry*; Schleyer, P. v. R., Ed.; Wiley-Interscience: New York, 1998.
(10) Bühl, M.; Kaupp, M.; Malkin, V. G.; Malkina, O. L. *J. Comput. Chem.* **1999**, *20*, 91.
(11) Schreckenbach, G.; Ziegler, T. *Theor. Chem. Acc.* **1998**, *2*, 71.
(12) Schreckenbach, G.; Ziegler, T. *J. Phys. Chem. A* **1997**, *101*, 3388.
(13) van Lenthe, E.; Baerends, E. J.; Snijders, J. G. *J. Chem. Phys.* **1993**, *99*, 4597.
(14) van Lenthe, E.; Wormer, P. E. S.; van der Avoird, A. *J. Chem. Phys.* **1997**, *107*, 2488.
(15) Jayatilaka, D. *J. Chem. Phys.* **1998**, *108*, 7587.
(16) (a) Salahub, D. R.; Fournier, R.; Mlynarski, P.; Papai, I.; St-Amant, A.; Ushio, J. In *Density Functional Methods in Chemistry*; Labanowski, J., Andzelm, J., Eds.; Springer: New York, 1991. (b) St-Amant, A.; Salahub, D. R. *Chem. Phys. Lett.* **1990**, *169*, 387.
(17) Malkin, V. G.; Malkina, O. L.; Eriksson, L. A.; Salahub, D. R. In *Modern Density Functional Theory: A Tool for Chemistry*; Seminario, J. M., Politzer, P., Eds.; Elsevier: Amsterdam, 1995; Vol. 2.
(18) Malkina, O. L.; Schimmelpfennig, B.; Kaupp, M.; Hess, B. A.; Chandra, P.; Wahlgren, U.; Malkin, V. G. *Chem. Phys. Lett.* **1998**, *296*, 93.
(19) Vaara, J.; Malkina, O. L.; Stoll, H.; Malkin, V. G.; Kaupp, M. Submitted.
(20) Schreckenbach, G. Ph.D. Thesis, The University of Calgary, Canada, 1996.
(21) Harriman, J. E. *Theoretical Foundations of Electron Spin Resonance*; Academic Press: New York, 1978.
(22) Malkin, V. G.; Malkina, O. L.; Casida, M. E.; Salahub, D. R. *J. Am. Chem. Soc.* **1994**, *116*, 5898.

present formulae are written in terms of a common gauge origin, the choice of individual-gauges-for-localized-orbitals (IGLO[43]) can be trivially read from the nuclear shielding formulae of ref 22.

As mentioned above, an accurate treatment of spin−orbit coupling is particularly critical for quantitative *g*-tensor calculations.[23] We base our implementation on our latest version of the deMon-NMR module for calculating the SO contribution to the nuclear shielding tensor[19] and use three different types of SO integrals in the present calculation: (1) from the full microscopic one- and two-electron SO Hamiltonian of eq 3 using the EAGLE code,[24] (2) from the effective one-electron one-center mean-field approximation for both one- and two-electron SO integrals[25] as implemented in the AMFI software,[26] and (3) from spin−orbit pseudopotentials of the Pitzer-Winter form.[27] The second alternative is a very accurate approximation of the first (as shown below), and allows calculations of much larger molecular systems due to eliminating the need to compute and store a large number of two-electron integrals. Since **g** is largely a valence property, SO-ECPs can be used to reduce the computational effort further by removing the core electrons and to take into account scalar relativistic effects when used in connection with Kohn−Sham valence pseudo-orbitals optimized in the presence of corresponding quasirelativistic ECPs. Furthermore, the implementation allows mixed usage of AMFI and SO-ECP integrals on different atomic centers of the molecule. Hence, it is possible to perform an atomic break-down of the calculated $\Delta\mathbf{g}_{SO/OZ}$ contributions.

To obtain a consistent account for all the important terms up to $O(\alpha^2)$, one has to additionally consider the bilinear terms of the Breit−Pauli Hamiltonian[21]

$$H_{RMC} = -\frac{1}{4}\alpha^2 g_e \sum_i p_i^2 \mathbf{s}_i \cdot \mathbf{B}_0 \tag{6}$$

the so-called kinetic energy correction to the spin−Zeeman interaction (taken up to $O(B_0)$, with $p = -i\nabla$), and the part of the SO Hamiltonian arising from the magnetic field dependence of the SO Hamiltonian (the $\mathbf{A}_0$-dependent terms in eq 3). After taking the appropriate expectation values, the former leads to a diagonal (isotropic) contribution

$$\Delta g_{RMC,uv} = -\frac{1}{2}\alpha^2 g_e \delta_{uv} \sum_{\mu\nu} P_{\mu\nu}^{\alpha-\beta} \langle \nu | p^2 | \mu \rangle \tag{7}$$

where

$$P_{\mu\nu}^{\alpha-\beta} = \sum_k^{occ(\alpha)} c_k^\mu c_k^{\nu *} - \sum_k^{occ(\beta)} c_k^\mu c_k^{\nu *} \tag{8}$$

is the spin density matrix in the atomic orbital (μ, ν) basis and *c* are the MO coefficients. The latter term causes diamagnetic gauge correction contributions, whose one-electron term reads

$$\Delta g_{GC(1e),uv} = \frac{1}{4}\alpha^2 g_e \sum_{\mu\nu} P_{\mu\nu}^{\alpha-\beta} \left\langle \nu \left| \sum_M \frac{\delta_{uv}(\mathbf{r}_M \cdot \mathbf{r}_O) - r_{M,u} r_{O,v}}{r_M^3} Z_M \right| \mu \right\rangle \tag{9}$$

In the present calculations we neglect the corresponding and analogous two-electron contribution $\Delta\mathbf{g}_{GC(2e)}$ due to its general smallness (see refs 7 and 12) and the lack of a computationally efficient approximation thereto.

3. Computational Details

3.1. Structures. For small main group radicals, we used for better comparison with the results of Schreckenbach and Ziegler (SZ) their DFT-optimized structures.[12] Similarly, we employed the DFT (VWN)-optimized structures of Patchkowski and Ziegler (PZ)[28] for a set of MXY_4^{m-} transition metal complexes. Most of the structures of 3d complexes are those reported in a recent study of hyperfine couplings for these systems[39] (mostly DFT-optimized, in a few cases experimental). Additional 3d complexes are the three vanadyl complexes [*N*,*N*′-ethylenebis(*o-tert*-butyl- *p*-methylsalicylaldiminato)]oxovanadium(IV), bis(*N*-isopropyl- *o*-methylsalicylaldiminato)oxovanadium(IV), and bis(*N*-methyl- *o-tert*-butyl-salicylaldiminato)oxovanadium(IV), for which experimental structures[29] were used. Structures of $Cu(acac)_2$ and $Cu(NO_3)_2$, and of phenoxyl radicals have been fully optimized with the Gaussian98 code,[30] at the gradient-corrected, unrestricted DFT level (BP86 functional[31,32]). Quasi-relativistic small-core pseudopotentials and (8s7p6d)/[6s5p3d] valence basis sets of the Stuttgart group were employed for the transition metals,[33,34] ECPs[35] with DZP valence basis sets[35−37] for main group atoms. A DZV basis[38] was used for hydrogen. The newly optimized structures are reported as Supporting Information.

3.2. *g*-Tensor Calculations. The Kohn−Sham calculations were performed in an unrestricted manner (UKS), using the deMon code,[16] with either local density (VWN[40]) or gradient-corrected (GGA) functionals. We mainly used BP86,[31,32] but PP86[32,41] and PW91[42] functionals were also tested. In most calculations, in particular in our comparison with the results of

(23) A consistent and complete incorporation of spin−orbit coupling into a Kohn−Sham framework is far from trivial. Thus, for example, spin−other−orbit terms arise strictly only from relativistic contributions to the electron−electron interaction. Rather than resorting to relativistic exchange-correlation potentials, we have in this work preferred to incorporate spin−orbit coupling explicitly via suitably chosen and well-established perturbation operators (see text).

(24) EAGLE is a code for the calculation of integrals of the Breit−Pauli SO Hamiltonian over molecular Cartesian Gaussian functions, written by P. Chandra and B. A. Hess.

(25) Hess, B. A.; Marian, C. M.; Wahlgren, U.; Gropen, O. *Chem. Phys. Lett.* **1996**, *251*, 365.

(26) Schimmelpfennig, B. *Atomic Spin−Orbit Mean-Field Integral Program*; Stockholms Universitet, Sweden, 1996.

(27) Pitzer, R. M.; Winter, N. W. *J. Phys. Chem.* **1988**, *92*, 3061.

(28) Patchkovskii, S.; Ziegler T. *J. Chem. Phys.* **1999**, *111*, 5730.

(29) Cornman, C. R.; Geiser-Bush, K. M., Rowley, S. P., Boyle, P. D. *Inorg. Chem.* **1997**, *36*, 6401.

(30) Frisch, M. J.; Trucks, G. W.; Schlegel, H. B.; Scuseria, G. E.; Robb, M. A.; Cheeseman, J. R.; Zakrzewski, V. G.; Montgomery, J. A. Jr.,; Stratmann, R. E.; Burant, J. C.; Dapprich, S.; Millam, J. M.; Daniels, A. D.; Kudin, K. N.; Strain, M. C.; Farkas, O.; Tomasi, J.; Barone, V.; Cossi, M.; Cammi, R.; Mennucci, B.; Pomelli, C.; Adamo, C.; Clifford, S.; Ochterski, J.; Petersson, G. A.; Ayala, P. Y.; Cui, Q.; Morokuma, K.; Malick, D. K.; Rabuck, A. D.; Raghavachari, K.; Foresman, J. B.; Cioslowski, J.; Ortiz, J. V.; Baboul, A. G.; Stefanov, B. B.; Liu, G.; Liashenko, A.; Piskorz, P.; Komaromi, I.; Gomperts, R.; Martin, R. L.; Fox, D. J.; Keith, T.; Al-Laham, M. A.; Peng, C. Y.; Nanayakkara, A.; Gonzalez, C.; Challacombe, M.; Gill, P. M. W.; Johnson, B.; Chen, W.; Wong, M. W.; Andres, J. L.; Gonzalez, C.; Head-Gordon, M.; Replogle, E. S.; Pople, J. A. *Gaussian 98*, revision A.7; Gaussian, Inc.: Pittsburgh, PA, 1998.

(31) Becke, A. D. *Phys. Rev. A* **1988**, *38*, 3098.

(32) Perdew, J. P. *Phys. Rev. B* **1986**, *33*, 8822.

(33) Andrae, D.; Häuβermann, U.; Dolg, M.; Stoll, H.; Preuss, H. *Theor. Chim. Acta* **1990**, *77*, 123.

(34) Dolg, M.; Wedig, U.; Stoll, H.; Preuss, H. *J. Chem. Phys.* **1987**, *86*, 866.

(35) Nicklaβ, A.; Dolg, M.; Stoll, H.; Preuss, H. *J. Chem. Phys.* **1995**, *102*, 8942. Bergner, A.; Dolg, M.; Küchle, W.; Stoll, H.; Preuss H. *Mol. Phys.* **1993**, *80*, 1431. Dolg, M. Ph.D. Dissertation, Universität Stuttgart, Germany, 1989.

(36) Kaupp, M.; Schleyer, P. v. R.; Stoll, H.; Preuss, H. *J. Am. Chem. Soc.* **1991**, *113*, 6012.

(37) d-Type polarization functions have been taken from: *Gaussian Basis Sets for Molecular Calculations*, Huzinaga, S., Ed.; Elsevier: New York, 1984.

(38) Godbout, N.; Salahub, D. R.; Andzelm J.; Wimmer, E. *Can. J. Chem.* **1992**, *70*, 560.

(39) Munzarová, M.; Kaupp, M. *J. Phys. Chem. A* **1999**, *103*, 9966.

(40) Vosko, S. H.; Wilk, L.; Nusair, M. *Can. J. Chem.* **1980**, *58*, 1200.

(41) Perdew, J. P.; Wang, Y. *Phys. Rev. B* **1986**, *33*, 8800.

(42) Perdew, J. P. *Physica B* **1992**, *172*, 1. Perdew, J. P. In *Electronic Structure of Solids '91*, Ziesche, P., Eschring, H., Eds.; Akademie Verlag: Berlin, 1991. Perdew, J. P.; Wang, Y. *Phys. Rev. B* **1992**, *45*, 13244.

SZ for simple main-group radicals and with those of PZ for some d^1 transition metal systems, we will concentrate on the BP86 results. The calculations were performed in two separate steps, (1) the Kohn−Sham SCF calculation, and (2) the computationally inexpensive perturbation calculation, based on the Kohn−Sham orbitals of the previous step. This two-step procedure makes it easy to alter the parameters of the perturbation calculation only, for example, to test different options to treat the gauge problem, different SO operators, or for analysis purposes.

As we employ exchange-correlation functionals that do not depend on the current density, the resulting perturbation calculations are uncoupled (UDFT). In NMR chemical shift calculations on main group compounds with low-lying excited states, it was found previously, that the simple correction term $\Delta E^{xc}_{k\rightarrow a}$ in eq 5 may be used to reduce the paramagnetic contributions to the shielding tensors, thereby improving in most cases the agreement with experiment.[17,22] In the case of the electronic *g*-tensor, we find that the accuracy of the experimental data available does typically not allow us to judge whether this SOS-DFPT correction term is beneficial to the agreement between theory and experiment. We will thus concentrate on the UDFT results and give SOS-DFPT results for comparison only in a few examples.

Unless noted otherwise, results are reported with the IGLO[43] choice of gauge. Orbitals were typically localized with the Boys procedure.[44] For the heavier main-group compounds and the square pyramidal d^1 complexes, the Pipek-Mezey localization[45] converged better and was used instead. The α and β MOs were localized separately. For analyses in terms of canonical MOs, a common gauge origin at the center of mass has been employed. *g*−Tensor calculations are known[6−8,12,14] to be less gauge-dependent than, for example, NMR chemical shift computations, and we find that the IGLO and common gauge results typically do not differ much.

All-electron basis sets used for the 3d metals were (15s11p6d)/[9s7p4d] sets designed previously for hyperfine calculations.[39] Basis sets for Mo and Zr were constructed from the primitive set of the well-tempered series of Huzinaga et al.[46] by removing the tightest three s-, two p- and four d-functions and adding the two most diffuse p-functions from the ECP basis set.[33] The resulting 24s19p13d sets were used fully uncontracted. Test calculations show that this allows a valid comparison with ECP results. The basis sets BII and BIII (also termed IGLO-II and IGLO-III) of Kutzelnigg et al.[43] (based on the earlier work of Huzinaga[47]) were used for main group atoms. In some cases, smaller DZVP basis sets[38] were also studied (either with or without p-polarization functions on hydrogen).

Energy-adjusted ECPs and valence basis sets for 4d and 5d transition metals were the same as those used in the structure optimizations,[33] augmented by appropriate spin−orbit pseudopotentials[33] in the perturbation step of the calculation. Similarly, an ECP treatment of main group atoms (mainly of Kr, Xe, and the halogens) employed the same quasirelativistic ECPs as the optimizations, together with SO-ECPs.[35] The valence basis sets were decontracted and extended to TZ + 2P quality. The fitting procedure of the SO-ECPs used differs slightly from that of the quasirelativistic ECPs, as they were obtained by a single-electron fit rather than by a multielectron fit.[33,35] Moreover, the SO-ECPs used in the present work have been fitted to two-component Wood-Boring or averaged four-component Dirac−Fock energies that do not include the Breit interaction. Thus, they do not cover the spin−other−orbit term. Development of improved two-component multielectron-fit ECPs and SO-ECPs adjusted to multiconfiguration Dirac−Fock−Breit energies is presently carried out by Stoll et al.,[48] and we plan to use these more accurate parameters in our future *g*-tensor work. In some cases we also used nonrelativistic ECPs in the Kohn−Sham step for interpretation purposes. Gauge factors arising from the use of ECPs in the IGLO treatment have been neglected in the present work.[49]

Table 1. Analysis of Different Contributions to *g*-Shifts (ppm) in CO^+ [a]

	exact SO treatment[b]		atomic mean-field appr.[c]		SZ[d]	
contribution	$\Delta g_{\|\|}$	$\Delta g_{\perp}$	$\Delta g_{\|\|}$	$\Delta g_{\perp}$	$\Delta g_{\|\|}$	$\Delta g_{\perp}$
$\Delta g_{GC(1e)}$	85	71	85	71	81	119
$\Delta g_{GC(2e)}$	-	-	-	-	−34	−61
Δg_{RMC}	−180	−180	−180	−180	−181	−181
$\Delta g_{SO/OZ(1e)}$	0	−3668	0	−3660	0	−3678
$\Delta g_{SO/OZ(2e)}$ (SSO[e], SOO[f])	0	1271	0	1312 (975[e], 337[f])	0	684
total[g]	−95	−2507	−95	−2458	−135	−3117

[a] UDFT results with BP86 functional. Our results with basis BIII and IGLO gauge. Results of SZ with STO basis and GIAO gauge. [b] Exact calculation of all SO integrals with the EAGLE code. [c] Atomic mean-field approximation. [d] Approximate treatment of two-electron SO terms.[12] [e] Spin−same−orbit contribution. [f] Spin−other−orbit contribution. [g] Gas-phase experiments give −2400 ppm for $\Delta g_{\perp}$.

4. All-Electron Calculations: The Importance of the Two-Electron SO Terms

For two systems, namely for CO^+ and for H_2O^+, SZ reported individual contributions to the Δg components from their DFT calculations.[12] This allows us detailed comparison, in particular regarding the different treatment of the two-electron SO terms ($\Delta g_{SO/OZ(2e)}$ terms). Table 1 gives the results for CO^+, Table 2 for H_2O^+. We give results with either (1) the exact (EAGLE) treatment of all one- and two-electron SO integrals, (2) the one-center and mean-field approximation (AMFI) to these integrals, and (3) the results of SZ, using their approximate treatment of the two-electron SO terms via an effective Kohn−Sham potential. In our mean-field SO calculations, we are furthermore able to separate the two-electron SO terms into contributions from spin−same−orbit (SSO) and spin−other−orbit (SOO) terms. This allows us to estimate the importance of the SOO terms, which were neglected in the approach of SZ. Note that, like SZ, we use the BP86 functional, that is, our calculations differ essentially only in the basis sets used (extended STO basis sets of SZ, extended GTO basis sets in our case), and in the treatment of the two-electron SO terms. The fact that we use IGLO rather than GIAO should not be relevant as we obtain essentially the same results with other choices of gauge origin.

(43) Kutzelnigg, W.; Fleischer, U.; Schindler, M. In *NMR-Basic Principles and Progress*; Diehl, P., Fluck, E., Günther, H.; Kosfeld, R., Eds.; Springer-Verlag: Heidelberg, 1990; Vol. 23, pp 165ff.

(44) Edmiston, C.; Ruedenberg, K. *Rev. Mod. Phys.* **1963**, *35*, 457. Edmiston, C.; Ruedenberg, K. *J. Chem. Phys.* **1965**, *43*, 597. See also: Boys, S. F. In *Quantum Theory of Atoms, Molecules and the Solid State*; Löwdin, P.-O., Ed.; Academic Press: New York, 1966; p 253. This prodecure is often incorrectly attributed to Foster, S.; Boys, S. F. *Rev. Mod. Phys.* **1963**, *35*, 457.

(45) Pipek, J.; Mezey, P. G. *J. Chem. Phys.* **1989**, *90*, 4916.

(46) Huzinaga, S.; Miguel, B. *Chem. Phys. Lett.* **1990**, *175*, 289. Huzinaga, S., Klobukowski, M. *Chem. Phys. Lett.* **1993**, *212*, 260.

(47) Huzinaga, S. *Approximate Atomic Functions*; University of Alberta, Canada, 1971.

(48) Metz, B.; Schweizer, M.; Stoll, H.; Dolg, M.; Liu, W. *Theor. Chem. Acc.* **2000**, *104*, 22.

(49) For a justification, see: Kaupp, M.; Malkin, V. G.; Malkina, O. L.; Salahub, D. R. *Chem. Phys. Lett.* **1995**, *235*, 382.

Table 2. Analysis of Different Contributions to *g*-Shifts (ppm) in H_2O^+ [a]

	atomic mean-field appr.[b,c]			SZ[d]		
contribution	Δg_{11}	Δg_{22}	Δg_{33}	Δg_{11}	Δg_{22}	Δg_{33}
$\Delta g_{GC(1e)}$	138	172	183	147	254	216
$\Delta g_{GC(2e)}$	-	-	-	−54	−109	−92
Δg_{RMC}	−312	−312	−312	−310	−310	−310
$\Delta g_{SO/OZ(1e)}$	28	5946	15993	0	6153	16808
$\Delta g_{SO/OZ(2e)}$ (SSO[e], SOO[f])	5 (10[e], −5[f])	−2104 (−1599[e], −505[f])	−5658 (−4300[e], −1358[f])	9	−1188	−3165
total[g]	−142	3702	10205	−209	4800	13457

[a] UDFT results with BP86 functional. Our results with basis BIII and IGLO gauge. Results of SZ with STO basis and GIAO gauge. [b] Mean-field and one-center approximation. [c] The exact treatment of the two-electron SO integrals with the EAGLE code gives the following results: $\Delta g_{11} = -142$ ppm, $\Delta g_{22} = 3855$ ppm, $\Delta g_{33} = 10422$ ppm. [d] Reference 12. [e] Spin−same−orbit contribution. [f] Spin−other−orbit contribution. [g] Gas-phase experiments give $\Delta g_{11} = 200$ ppm, $\Delta g_{22} = 4800$ ppm, $\Delta g_{33} = 18800$ ppm.

We first note that the agreement between the exact (EAGLE) treatment and the one-center mean-field approximation (AMFI) is excellent, both for the $\Delta g_{SO/OZ(1e)}$ terms (which include the one-center approximation in AMFI but not in EAGLE), and for the $\Delta g_{SO/OZ(2e)}$ terms. Differences are below 7% (typically below 5%) in the two-electron terms, that is, much less for the overall *g*-shifts. This confirms the excellent performance of the atomic mean-field SO approximation, as found in many other types of applications.[18,25,50] For systems with heavier atoms, the mean-field approximation is expected to be even more accurate. The computational effort for the atomic mean-field approximation is not much more than for the one-electron SO integrals alone. Therefore, this approach removes effectively any SO-integral bottleneck from our calculations with very little sacrifice in the accuracy, and it enables us to treat large systems.

As shown already by other workers (see, e.g., refs 6 and 7), the *g*-shift tensors are usually−except for very light systems or for very small components−dominated by the second-order (paramagnetic) $\Delta g_{SO/OZ(1e)}$ and $\Delta g_{SO/OZ(2e)}$ terms, while the first-order (diamagnetic) contributions (Δg_{RMC} and $\Delta g_{GC(1e)}$ terms) are small. In both CO^+ and H_2O^+, our Δg_{RMC} terms agree quantitatively with the results of SZ. Similarly, the Δg_{RMC} contributions for these two radicals, as well as for NO_2 and MgF, agree excellently with the MRCI results of Lushington.[7] The $\Delta g_{GC(1e)}$ corrections are not directly comparable, due to the different choice of gauge origin. Nevertheless, they are close to the results of SZ and agree also with those of Lushington (we find an even better agreement when using a common gauge origin at the center of mass). We neglect the $\Delta g_{GC(2e)}$ corrections. They have been found to be smaller and of the opposite sign to the $\Delta g_{GC(1e)}$ terms, that is, small compared to the paramagnetic terms.[7,12] This is expected to cause slight errors for very small components, where the spin−orbit terms are small, but it will not influence much the comparison with experiment.

Interestingly, even the $\Delta g_{SO/OZ(1e)}$ contributions to the larger components agree with the results of SZ to within better than 5%. Thus, any significant deviation between the overall results must stem from the treatment of the $\Delta g_{SO/OZ(2e)}$ terms. Indeed, in both systems the two-electron SO contributions recovered by SZ account for only ∼50% of our results. As a consequence, the overall *g*-shifts of SZ are generally somewhat larger than ours, as the partial compensation of the one-electron SO terms by the two-electron terms is underestimated. We have tried to find out to what extent the incomplete recovery of the two-electron terms by SZ is due to either (1) the neglect of the SOO terms or (2) to the approximations involved in the effective Kohn−Sham potential used. Tables 1 and 2 show that in both systems, the SOO term accounts for ∼25% of the total $\Delta g_{SO/OZ(2e)}$ terms. Thus, about half of the errors of SZ in the two-electron terms is due to the neglect of the SOO term, the other half must be due to the other approximations mentioned.

Table 3. *g*-Tensor Components (ppm) for Some Light Main Group Radicals[a]

		this work[b]	SZ[c]	Lushington (MRCI)[d]	exp.[e]	
H_2O^+	Δg_{11}	−142	103	−292	200	gas phase
	Δg_{22}	3702	5126	4217	4800	
	Δg_{33}	10205	13824	16019	18800	
CO^+	$\Delta g_{\perp}$	−2458	−3129	−2674	−2400	gas phase
	$\Delta g_{\parallel}$	−93	−138	−178	-	
HCO	Δg_{11}	−224	−270		0	matrix
	Δg_{22}	2275	2749		1500	
	Δg_{33}	−7476	−9468		−7500	
C_3H_5	Δg_{11}	−65	−115		0	matrix
	Δg_{22}	497	660		400	
	Δg_{33}	603	769		800	
NO_2	Δg_{11}	−688	−760	−235	−300	gas phase
	Δg_{22}	3400	4158	3806	3900	
	Δg_{33}	−11229	−13717	−10322	−11300	
NF_2	Δg_{11}	−617	−738		−100	matrix
	Δg_{22}	3928	4678		2800	
	Δg_{33}	6288	7619		6200	
MgF	$\Delta g_{\perp}$	−1869	−2178	−1092	−1300	matrix
	$\Delta g_{\parallel}$	14	−60	−59	−300	

[a] UDFT-BP86 results. [b] Basis BIII, UDFT-IGLO, AMFI approximation. [c] UDFT-GIAO.[12] [d] Multireference configuration interaction results.[7] [e] Experimental data as quoted in refs. 7,12.

Table 3 compares our overall calculated *g*-shift components for some small, light main-group compounds to the DFT results of SZ, the CI data of Lushington et al., and experiment (either in the gas phase or in matrix). As expected from the above discussion, our *g*-shift components are generally of smaller absolute value than those of SZ, due to the more complete treatment of the two-electron SO terms. As SZ's results often overestimate the absolute values of the experimental *g*-shift components, in the majority of cases our data are overall in somewhat closer agreement with experiment (exceptions are Δg_{33} of H_2O^+ and C_3H_5, where the experimental value is higher). Figure 1 compares graphically our UDFT-BP86 data for light main-group systems to experiment. The plot includes the data from Table 3 and those for the larger substituted aromatic radicals discussed in section 6. The agreement is reasonable. A notable exception is Δg_{33} of H_2O^+. The MRCI results of Lushington are in much better agreement with experiment. The H_2O^+ radical cation may be a particularly difficult case for a Kohn−Sham approach, due to the near-degeneracy between HOMO and SOMO.

(50) See, for example: Ruud, K.; Schimmelpfennig, B.; Ågren, H. *Chem. Phys. Lett.* **1999**, *310*, 215. Maron, L.; Leininger, T.; Schimmelpfennig, B.; Vallet, V.; Heully, J.-L.; Teichteil, Ch.; Gropen, O.; Wahlgren, U. *Chem. Phys. Lett.* **1999**, *244*, 195. Fagerli, H.; Schimmelpfennig, B.; Gropen, O.; Wahlgren, U. *THEOCHEM* **1998**, *451*, 227.

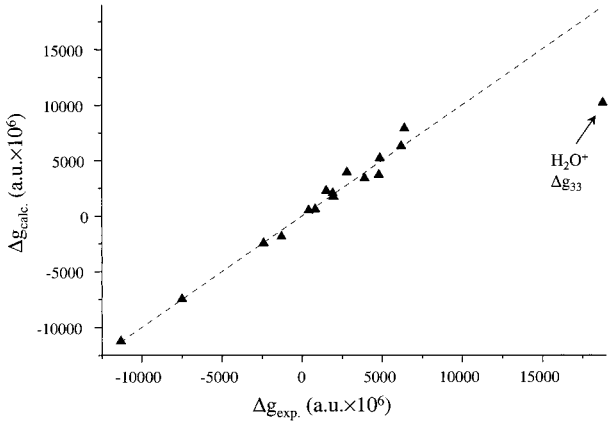

Figure 1. Comparison of calculated and experimental *g*-shift tensor components (ppm) for first-row compounds (cf. Tables 3, 9; Only components with $|\Delta g| > 1000$ ppm have been included).

Obviously, the importance of errors in the two-electron SO terms for the overall *g*-shifts depends on the relative importance of the $\Delta g_{SO/OZ(2e)}$ contributions. In CO^+ and H_2O^+, the two-electron terms amount to ~35% of the absolute magnitude of the $\Delta g_{SO/OZ(1e)}$ terms (with opposite sign). We find this to be the general behavior for compounds containing atoms from at most the second period. Our results for other systems containing heavier main group atoms indicate that the importance of the two-electron terms decreases to ~20%, 10%, 7% for the third, fourth and fifth period, respectively (see, e.g., results for CF_3X^-; X = Cl, Br, I, in Table 4). The same percentages were found previously in both DFT[18] and MCSCF calculations[51] of SO corrections to NMR chemical shifts. Thus, the accurate treatment of the two-electron terms becomes somewhat less important for compounds of heavier main group elements. For light main group, for example, organic radicals, the two-electron SO terms are particularly critical. The SOO term accounts for ~20% of the two-electron SO terms also for the heavier main group compounds (cf. Table 4).

The relative importance of the different terms changes when transition metals are involved. This is demonstrated for the simple 3d and 4d complexes TiF_3 and ZrH_3 in Table 5. In both cases, the spin density is mainly localized on the metal, and the SO coupling at the metal dominates the *g*-tensor. For the titanium complex, the $\Delta g_{SO/OZ(2e)}$ contributions amount to ~47% and ~55% of the magnitude of the $\Delta g_{SO/OZ(1e)}$ terms for $\Delta g_{||}$ and $\Delta g_{\perp}$, respectively. For the ZrH_3 4d model complex the fractions are ~34% and ~31%, respectively. In both cases, the two-electron contributions are thus of considerably larger relative importance than with main group elements of the same row (cf. ~13% for Br, ~7% for I). This is probably related to the more pronounced penetration of the valence d-orbitals of the transition metals into the core.[52]

Another difference compared to the main group case is seen with the SOO term, which for both TiF_3 and ZrH_3 accounts for only ~10−12% of the $\Delta g_{SO/OZ(2e)}$ contribution, that is, it is only about half as important as in the main group cases we have looked at above. Good agreement with the perturbational UKS results (obtained with the SZ code) of van Lenthe et al.[14] for TiF_3 may be obtained by reducing our $\Delta g_{SO/OZ(2e)}$ contributions by ~50%. This suggests that the main difference is in their incomplete treatment of the two-electron terms. On the other hand, their restricted Kohn−Sham (ROKS) calculations (both perturbational and two-component treatment) give much larger $\Delta g_{\perp}$ than the UKS treatment, i.e., spin polarization does seem to be important. Here the ROKS data are closer to experiment, probably due to error compensation, cf. section 6.

The previous examples were relatively simple, as the spin−orbit coupling arose mainly from one (the heaviest) atom, and from only a few molecular orbitals. Obviously, things may be much more complicated, if several heavy atoms are involved, and if several MOs may contribute. As an illustration, Table 6 compares the analyses for the two square pyramidal complexes $CrOF_4^-$ and $CrOCl_4^-$. In the case of $CrOF_4^-$, things are still relatively straightforward. The $\Delta g_{SO/OZ(2e)}$ terms amount to about half of the $\Delta g_{SO/OZ(1e)}$ terms (~51% for $\Delta g_{||}$, ~45% for $\Delta g_{\perp}$), and the SOO term to about 11−14% of the $\Delta g_{SO/OZ(2e)}$ contribution. However, in the case of $CrOCl_4^-$, $\Delta g_{\perp}$ behaves "normally" (~45% magnitude of the two-electron terms, ~10% fraction of SOO terms), but $\Delta g_{||}$ is atypical. Here the $\Delta g_{SO/OZ(2e)}$ terms are very small (~2%; with ~35% SOO contribution). An MO analysis (section 7) indicates that at least two occupied MOs contribute significantly to $\Delta g_{||}$, with opposite signs. The

Table 4. Analysis of Different Contributions to *g*-Shifts (ppm) in CF_3X^- (X = Cl, Br, I)[a]

CF_3Cl^-		$\Delta g_{||}$	$\Delta g_{\perp}$
all-el.[a]	$\Delta g_{GC(1e)}$	130	96
	Δg_{RMC}	−315	−315
	$\Delta g_{SO/OZ(1e)}$	−482	17891
	$\Delta g_{SO/OZ(2e)}$	134	−3474
	(SSO[b], SOO[c])	(93[b], 41[c])	(−2768[b], −707[c])
total all-el.[a]		−532	14198
ECP-QR(Cl)[d]		−390	12961
SZ NR[e,f]		−609	14573
SZ QR[e,g]		−610	15112
exp.[h]		−200	4700
CF_3Br^-		$\Delta g_{||}$	$\Delta g_{\perp}$
all-el.[a]	$\Delta g_{GC(1e)}$	167	401
	Δg_{RMC}	−313	−313
	$\Delta g_{SO/OZ(1e)}$	−475	57833
	$\Delta g_{SO/OZ(2e)}$	151	−5663
	(SSO[b], SOO[c])	(117[b], 34[c])	(−4583[b], −1080[c])
total all-el.[a]		−470	52258
ECP-QR(Br)[d]		−353	53680
SZ NR[e,f]		−635	67273
SZ QR[e,g]		−637	70229
exp.[h]		−1300	18900
CF_3I^-		$\Delta g_{||}$	$\Delta g_{\perp}$
all-el.[a]	$\Delta g_{GC(1e)}$	196	−56
	Δg_{RMC}	−303	−303
	$\Delta g_{SO/OZ(1e)}$	−452	137144
	$\Delta g_{SO/OZ(2e)}$	112	−9455
	(SSO[b], SOO[c])	(76[b], 36[c])	(−7833[b], − 1622[c])
total all-el.[a]		−447	127330
ECP-QR(I)[d]		−291	138056
SZ NR[e,f]		−581	146759
SZ QR[e,g]		−571	161466
exp.[h]		−2100	46000

[a] UDFT-IGLO results with BP86 functional and AMFI approximation. All-electron results with basis BII. [b] Spin−same−orbit terms only. [c] Spin−other−orbit terms only. [d] Quasirelativistic ECP/SO-ECP and TZ+2P valence basis on all halogen atoms, BII on C. [e] DFT-GIAO, ref 12. [f] Without scalar relativistic effects. [g] With scalar relativistic effects included. [h] In tetramethylsilane matrix (Hasegawa, A.; Williams, F. *Chem. Phys. Lett.* **1977**, *46*, 66). These anions are expected to experience increasing interactions with the environment from X = Cl through X = I. Therefore, the experimental data are probably not well-suited to be compared with calculations on the isolated anions.

(51) Vaara, J.; Ruud, K.; Vahtras, O.; Ågren, H.; Jokisaari, J. *J. Chem. Phys.* **1998**, *109*, 1212.

(52) The fact that the 3d shell is the first shell with $l = 2$ and thus particularly compact, may be responsible for the particularly large $\Delta g_{SO/OZ(2e)}$ contributions for 3d systems (similar arguments apply to the 2p shell).

Table 5. Analysis of Different Contributions to *g*-Shifts (ppm) in TiF_3 and ZrH_3[a]

	TiF_3		ZrH_3	
contribution	$\Delta g_{\|\|}$	$\Delta g_{\perp}$	$\Delta g_{\|\|}$	$\Delta g_{\perp}$
$\Delta g_{GC(1e)}$	+203	+371	+227	+484
Δg_{RMC}	−320	−320	−255	−255
$\Delta g_{SO/OZ(1e)}$	−1924	−58669	−6007	−250046
$\Delta g_{SO/OZ(2e)}$	+907	+32043	+2037	+77658
(SSO[b], SOO[c])	(+783[b], +124[c])	(+28199[b], +3844[c])	(+1833[b], +204[c])	(+69864[b], +7795[c])
total all-el.	−1124	−26577	−3998	−172160
ECP-NR(Zr)[d]			−3377	−160070
ECP-QR(Zr)[e]			−2673	−146534
van Lenthe UKS[f]	−1700	−42800		
van Lenthe ROKS[g]	+100	−73300		
van Lenthe 2-comp.[h]	−1000	−79700		
exp.	−11100[i]	−111900[i]		
	−3700[j]	−123700[j]		

[a] Present all-electron calculations at UDFT-IGLO level. The AMFI approximation, 9s7p4d basis on Ti, 24s19p13d basis on Zr, and BII on H, BIII on F. [b] Spin−same-orbit contribution. [c] Spin−other-orbit contribution. [d] Nonrelativistic ECP in the KS calculation. [e] Quasirelativistic ECP in the KS calculation. [f] Reference 14. With the perturbational approach of SZ, unrestricted KS wave function. [g] Reference 14. With the perturbational approach of SZ, restricted KS wave function. [h] Reference 14. Two-component ZORA calculation, spin-restricted. [i] Average of two sites in Ne matrix.[62] [j] Ar matrix result.[62]

Table 6. Analysis of Different Contributions to *g*-Shifts (ppm) in $CrOF_4^-$ and $CrOCl_4^-$ [a]

	$CrOF_4^-$		$CrOCl_4^-$	
contribution	$\Delta g_{\|\|}$	$\Delta g_{\perp}$	$\Delta g_{\|\|}$	$\Delta g_{\perp}$
$\Delta g_{GC(1e)}$	+549	+472	+505	+482
Δg_{RMC}	−701	−701	−657	−657
$\Delta g_{SO/OZ(1e)}$	−27513	−39331	+20900	−32848
$\Delta g_{SO/OZ(2e)}$	+14073	+17741	−407	+14955
(SSO[b], SOO[c])	(+12471[b], +1602[c])	(+15216[b], +2525[c])	(−266[b], −141[c])	(+13399[b], +1556[c])
total	−13592	−21811	+20341	−18067
PZ[d]	−19000	−29000	+18000	−21000
exp.[e]	−43000	−34000	−10000	−25000

[a] UDFT-IGLO results with BP86 functional. AMFI approximation, 9s7p4d basis on Cr, BII on all other atoms. [b] Same-orbit contribution. [c] Other-orbit contribution. [d] UDFT-GIAO results, ref 28. Data given only in ppt accuracy. [e] Experimental references as compiled in ref 28.

$\Delta g_{SO/OZ(2e)}$ contributions from these two MOs compensate each other to a large extent. Thus, obviously the importance of the two-electron terms, as well as the relative contributions from the SSO and SOO terms to them may differ significantly from system to system, and for different tensor components within one system. It is therefore not justified to use a simple scaling procedure to correct for a neglect of certain two-electron SO terms.

We may again ask to what extent the differences of our results relative to those of Ziegler et al. are due to their incomplete treatment of the $\Delta g_{SO/OZ(2e)}$ terms. If we simply reduce our two-electron terms by half, we obtain roughly −20000 ppm and −30000 ppm for $\Delta g_{||}$ and $\Delta g_{\perp}$, respectively, in $CrOF_4^-$, in much better agreement with the results of Patchkovski and Ziegler.[28] The same procedure applied to $CrOCl_4^-$ produces more negative $\Delta g_{\perp}$ (∼−25000 ppm), whereas $\Delta g_{||}$ is not affected much, due to the smallness of the two-electron terms in this case.

5. ECP Calculations: Validation of Spin−Orbit Pseudopotentials

Table 7 compares all-electron (AE) and pseudopotential (ECP/SO-ECP) treatments of Δg components for NF_2, KrF, XeF, and $MoOF_4^-$. Table 3 includes the same comparison for CF_3X^- (X = Cl, Br, I), and Table 5 for ZrH_3. The results of Ziegler et al., with an approximate treatment of the $\Delta g_{SO/OZ(2e)}$ terms, are included in Tables 4 and 7 as well, and experimental data are given for completeness. However, at least the data for KrF, XeF, and particularly those for the anions CF_3X^-, are probably influenced significantly by environmental effects (cf. below). We will thus only compare the different theoretical approaches. For easier comparison, the ECP calculations use ECPs and SO-ECPs only for the heaviest atoms, whereas the all-electron AMFI treatment is kept for the lighter atoms (as discussed in section 2, this combination of methods is allowed, due to the atomic nature of the SO operators involved).

As the SO-ECPs used here have been adjusted to atomic calculations that did not include the Breit interaction, they do not cover the SOO term. The ECP results might therefore be expected to slightly overestimate the $\Delta g_{SO/OZ}$ contributions, typically by ∼10−15% for NF_2, by less than half of this for the heavier main group and transition metal species (cf. section 4). On the other hand, the direct comparison between all-electron and ECP−NR results has to be viewed with some caution, as the use of nonrelativistic ECPs with the relativistically adjusted SO-ECPs is not completely consistent.

Inspecting the data of Tables 5 and 7, the ECP−NR results are found to be both high or low relative to the all-electron data. However, agreement is found generally within a few percent. The differences are significantly smaller than, for example, differences between local or gradient-corrected density functionals, and also smaller than differences relative to the approximate treatment of the SO integrals by SZ. This indicates that the combination of ECPs in the Kohn−Sham step with SO-ECPs in the perturbation treatment provides a useful valence-only approximation to the all-electron calculations. In all cases, our *g*-shifts are lower than those of SZ.

Comparison of the ECP−NR and ECP-QR results for KrF and XeF (Table 7) suggests an increase of $\Delta g_{\perp}$ due to scalar

Table 7. Comparison of All-Electron and ECP/SO-ECP Results for *g*-Shift Components (ppm)[a]

		Δg_{11}	Δg_{22}	Δg_{33}
NF_2	all-el.[b]	−617	3928	6288
	ECP-QR(F)[c]	−774	3980	6699
	SZ[d]	−738	4678	7619
	exp.[e]	−100	2800	6200
			$\Delta g_{\parallel}$	$\Delta g_{\perp}$
KrF	all-el.[b]		−246	49494
	ECP-NR(Kr)[f]		−166	48303
	ECP-QR(Kr)[f]		−164	50857
	SZ NR[d,g]		−335	60578
	SZ QR[d,h]		−345	61851
	exp.[e]		−2000	66000
XeF	all-el.[b]		−184	127288
	ECP-NR(Xe)[f]		−91	130003
	ECP-QR(Xe)[f]		−93	134302
	SZ NR[d,g]		−340	151518
	SZ QR[d,h]		−346	158083
	exp.[e]		−28000	124000
$MoOF_4^-$	all-el.[b]		−51855	−46733
	ECP-NR(Mo)[f]		−48633	−47293
	ECP-QR(Mo)[f]		−50557	−47646
	PZ QR[i]		−62000	−57000
	exp.[j]		−167000	−76000

[a] UDFT-IGLO results with BP86 functional and AMFI approximation. [b] All-electron basis sets 24s19p13d for Mo, BIII basis for F in NF_2, KrF, XeF, BII for all other atoms. [c] ECP and TZ+2P valence basis on F, BII on N. [d] Reference 12. [e] As cited in ref 12. [f] Nonrelativistic and quasi-relativistic ECP, respectively, on the heavy atom, with all-electron treatment for the light atoms. [g] Non-relativistic. [h] With scalar relativistic effects included. [i] Reference 28. [j] Sunil, K. K.; Rogers, M. T. *Inorg. Chem.* **1981**, *20*, 3283.

relativistic effects (more so for XeF than for KrF). This is consistent with the increase of the *g*-shifts upon inclusion of scalar relativistic effects by SZ (at the first-order Breit-Pauli level). Moreover, the relative increase is of comparable magnitude, suggesting that the comparison of NR-ECP and QR-ECP results provides a reasonable estimate of the influence of scalar relativistic effects.

In the case of the anions CF_3X^- (X = Cl, Br, I; Table 4), the ECP calculations use quasirelativistic ECPs and SO-ECPs for X (no appropriate nonrelativistic ECPs have been available for comparison). The QR-ECP results for $\Delta g_{\perp}$ in CF_3Cl^- are ∼9% lower than the all-electron results. In contrast, the QR-ECP calculations give ∼3% and ∼8% larger values for CF_3Br^- and CF_3I^-, respectively, probably in part due to the inclusion of scalar relativistic effects in the ECP calculations (cf. comparison between nonrelativistic and relativistic results of SZ). Again, our $\Delta g_{\perp}$ components are somewhat smaller than those of SZ. The experimental data were obtained in a solid matrix of tetramethylsilane and are probably not strictly comparable to the free-anion calculations. The increasing discrepancy from X = Cl through X = I may be due either (1) to potential problems with the perturbation treatment of SO coupling for the heavier halogens, as suggested by SZ, or (2) to an increasingly diffuse nature of the SOMO (which corresponds to a σ^* (C−X) MO and does exhibit small positive energies in our Kohn−Sham calculations) and thus increasing interactions with the environment. The second possibility, which we find more likely, could be tested by calculations that simulate the matrix environment. This is beyond the scope of the present study.

ECP and all-electron results for the 4d model system ZrH_3 may be compared in Table 5. The ECP−NR calculations give ∼7% too positive $\Delta g_{\perp}$. Scalar relativistic effects appear to reduce further significantly the absolute value. In contrast, for the more complicated 4d complex $MoOF_4^-$ (Table 7), the scalar relativistic effects appear to be modest.

Table 8. Comparison of First-Order Corrections (ppm) from All-Electron and ECP/SO-ECP Calculations[a]

		Δg_{RMC}	$\Delta g_{GC(1e)}$[b]
NF_2	all-el. NR	−314	126,232,225
	ECP-QR(F)	−316	127,233,226
KrF	all-el. NR	−429	179,491
	ECP-NR(Kr)	−351	170,472
	ECP-QR(Kr)	−349	170,473
XeF	all-el. NR	−414	228,598
	ECP-NR(Xe)	−303	211,567
	ECP-QR(Xe)	−304	209,569
CF_3Cl^-	all-el. NR	−315	144,82
	ECP-QR(Cl)	−244	135,59
CF_3Br^-	all-el. NR	−313	181,200
	ECP-QR(Br)	−229	170,179
CF_3I^-	all-el. NR	−303	212,293
	ECP-QR(I)	−209	195,270
ZrH_3	all-el. NR	−247	251,455
	ECP-NR(Zr)	−118	220,421
	ECP-QR(Zr)	−117	219,419
$MoOF_4^-$	all-el. NR	−555	797,531
	ECP-NR(Mo)	−283	715,472
	ECP-QR(Mo)	−278	708,470

[a] UDFT-BP86 results. Basis sets and ECPs as in Tables 3, 5, and 7. $\Delta g_{GC(1e)}$ terms with common gauge at center of mass. [b] Δg_{11}, Δg_{22}, and Δg_{33} for NF_2, $\Delta g_{\parallel}$ and $\Delta g_{\perp}$ for the other compounds.

Table 8 compares Δg_{RMC} contributions obtained with all-electron and ECP approaches. While the agreement is excellent for the light NF_2 molecule, the ECP results increasingly underestimate the all-electron results for increasingly heavy atoms. It appears that the ECP calculations miss some core−shell contributions to this term. However, in view of the dominance of SO terms, errors in the Δg_{RMC} term will typically introduce only negligible errors in the overall computed *g*-shifts. The $\Delta g_{GC(1e)}$ contributions are more difficult to compare directly, due to their gauge dependence. Table 8 includes results with a common gauge at the center of mass. Again, it seems that the ECP calculations underestimate these terms moderately for the heavier systems, whereas the core contribution from the fluorine 1s-orbitals in NF_2 apparently is negligible.

6. Further Validation Calculations

In this section, we validate the performance of the present DFT approach for a somewhat larger set of species, including also larger main group and transition metal systems. Table 9 gives *g*-shift tensors for some phenoxyl radicals (see Scheme 1), which have received appreciable attention due to the paramount importance of the tyrosyl radical in biological systems.[53] In addition to the free, unsubstituted phenoxyl radical, for which no experimental data appear to be available, we have also studied the substituted 2,4,6-tris- *t*-Bu-C_6H_2O radical, as well as the tyrosyl radical itself. The *g*-tensor of the tyrosyl radical has been studied by semiempirical calculations,[4] but to our knowledge not by first-principles methods. We have used the neutral rather than the zwitter-ionic form of the amino acid residue.

We take the parent phenoxyl radical as an example to test the basis set dependence of the DFT results, and to compare different exchange-correlation functionals (Table 9). The Δg_{22}

(53) See, for example: (a) Ivancich, A.; Mattioli, T. A.; Un, S. *J. Am. Chem. Soc.* **1999**, *121*, 5743. (b) Allard, P.; Barra, A. L.; Andersson, K. K.; Schmidt, P. P.; Atta, M.; Gräslund, A. *J. Am. Chem. Soc.* **1996**, *118*, 895. (c) van Dam, P. J.; Willems, J.-P.; Schmidt, P. P.; Pötsch, S.; Barra, A.-L.; Hagen, W. R.; Hoffman, B. M.; Andersson, K. K.; Gräslund, A. *J. Am. Chem. Soc.* **1998**, *120*, 5080.

Table 9. Effects of Basis Sets and Functionals on Computed *g*-Shift Components (ppm) for Phenoxyl Radicals[a]

	basis	Δg_{iso}	Δg_{11}	Δg_{22}	Δg_{33}
		phenoxyl			
VWN, UDFT	DZVD[b]	3156	−139	363	9243
VWN, UDFT	DZVP	4429	−150	2145	11292
VWN, UDFT	BII	4505	−85	2249	11351
VWN, UDFT	BIII	4543	−83	2292	11419
PP86, UDFT	BII	3388	−91	2125	8130
PW91, UDFT	BII	3548	−89	2117	8617
BP86, UDFT	DZVD[b]	2333	−146	319	6825
BP86, UDFT	DZVP	3355	−160	2031	8194
BP86, UDFT	BII	3405	−91	2117	8188
BP86, UDFT	BIII	3461	−85	2170	8299
BP86, SOS-DFPT[c]	BIII	2980	−85	2133	6891
ROHF[d]	cc-pVDZ	24200	100	5200	67400
MCSCF[d]	cc-pVDZ	2500	200	2400	5000
		t-Bu-substituted phenoxyl[e]			
VWN, UDFT	DZVP	2721	42	1834	6285
BP86, UDFT	DZVP	2314	−4	1734	5213
BP86, SOS-DFPT[c]	DZVP	2093	−7	1721	4565
exp.		2297	70	1960	4860
		tyrosyl			
VWN, UDFT	DZVP	4263	−167	2177	10480
BP86, UDFT	DZVP	3264	−181	2064	7908
BP86, SOS-DFPT[c]	DZVP	2827	−195	2037	6639
exp. (*E. coli* RNR)[f]		2670	−300	1900	6400
exp. (*S. typh.* RNR)[g]		2848 (±70)	−200	2000	6600
exp. (*N*−Ac-L-TyrO)[h]		3200 (±200)			7000 (±200)

[a] DFT results with IGLO gauge and AMFI approximation. [b] Without polarization functions on hydrogen. [c] Including correction term in Loc.1 approximation. [d] Results with common gauge at center of mass.[54] Only a limited number of digits were given. [e] Results for 2,4,6-tris-*t*-Bu-C_6H_2O. Experimental data in frozen toluene solution (145 K) from Bresgunov, A. Y.; Dubinsky, A. A.; Poluektov, O. G.; Lebedev, Y. S.; Prokov'ev, A. I. *Mol. Phys.* **1992**, *75*, 1123. [f] Experimental data for the tyrosyl radical in *E. coli* RNR. (Hoganson, C. W.; Sahlin, M.; Sjöberg, B.-M.; Babcock, G. T. *J. Am. Chem. Soc.* **1996**, *118*, 4672; see also ref 4). [g] Experimental data for the tyrosyl radical in *S. typhimurium* RNR (ref 53 b). [h] Irradiated crystal of *N*-acetyl-L-tyrosine (Mezzetti, A.; Maniero, A. L.; Brustolon, M.; Giacometti, G.; Brunel, L. C. *J. Phys. Chem. A* **1999**, *103*, 9636).

Scheme 1. Three Phenoxyl Radicals Studied

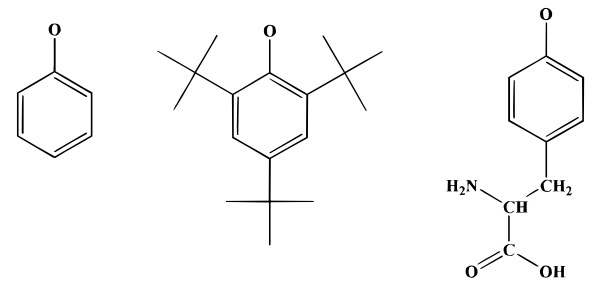

phenoxyl 2,4,6-tris-*t*-Bu-phenoxyl tyrosyl

and Δg_{33} components change relatively little in going from DZVP to the larger BII and BIII basis sets (this holds for both VWN and BP86 functionals). Only the DZVD basis, that is, omission of polarization p-functions on hydrogen, leads to a rather dramatic deterioration of the results, mainly for Δg_{22}. Closer inspection indicates that without the polarization functions, too much spin density is accumulated on the hydrogen atoms and withdrawn from the heavy atoms. In going from the local VWN to the gradient-corrected BP86 functional, the *g*-shifts decrease moderately but nonnegligibly. On the other hand, differences between different GGA functionals (BP86, PP86, PW91) are small. This is our general experience and the reason for concentrating mostly on one functional (BP86) throughout this work. An only modest dependence on the functional was also noted by Ziegler and co-workers,[12,28] and similar conclusions pertain to NMR chemical shift calculations on main-group nuclei.[17]

We may compare our results for the phenoxyl radical to the ROHF and MCSCF calculations of Engström et al.[54] They found that electron correlation is extremely important for the description of the *g*-tensor of the phenoxyl radical. This may be seen from the dramatically overestimated Δg_{22} and Δg_{33} components at the ROHF level (Table 9). Much lower *g*-shifts were obtained at the MCSCF level (Table 9). Our DFT results (e.g., UDFT-IGLO with BP86 functional and BIII basis) are much closer to the MCSCF than to the ROHF data but give ∼65% larger Δg_{33} than the former.

The good agreement with the experimental result for the 2,4,6-tris- *t*-Bu-C_6H_2O radical has been taken as evidence for the good quality of the CASSCF wave function for the phenoxyl radical.[54] While the substituted radical was too large to be studied at the MCSCF level, our DFT approach is easily applicable also to the larger system. Interestingly, the computed *g*-shifts are considerably reduced by the substitution (Table 9). In particular, Δg_{33} is much lower. On the other hand, our computed results for the tyrosyl radical are much closer to those for the unsubstituted phenoxyl radical. *tert*-Butyl substituents in ortho position have obviously a rather significant effect on the spin density within the system (in particular on that for oxygen, which dominates the *g*-tensor; cf. below), but the amino acid moiety in para position of the tyrosyl radical oxygen atom affects the spin density distribution much less. Thus, while the free phenoxyl radical is not a very good model to study quantitatively the *g*-tensor of the 2,4,6-tris-*t*-Bu-C_6H_2O radical, it serves as a very good model for the biologically relevant tyrosyl system (as previously concluded from spin-density calculations[55]). Notably, the present DFT approach reproduces rather accurately the experimental differences between the two substituted radicals. This suggests that substituent influences on the *g*-tensor in aromatic radicals may now be studied with good accuracy. We note in passing that, in contrast to the ring

(54) Engström, M.; Vahtras, O.; Ågren, H. *Chem. Phys.* **1999**, *243*, 263.

(55) Qin, Y.; Wheeler, R. A. *J. Am. Chem. Soc.* **1995**, *117*, 6083.

protons, the neglect of polarization p-functions on the *t*-butyl hydrogen atoms in the 2,4,6-tris-*t*-Bu-C_6H_2O radical has a negligible effect on the computed *g*-shifts.

In addition to our UDFT-IGLO results with various functionals and basis sets, Table 9 also includes SOS-DFPT results with the BP86 functional. As is well-known from NMR chemical shift calculations, the SOS-DFPT correction term reduces to some extent the paramagnetic contributions and thus the overall shift components.[17,22,56] No experimental data are available to judge the performance of the different approaches for the free phenoxyl radical. For the 2,4,6-tris- *t*-Bu-C_6H_2O radical, the UDFT and SOS-DFPT results with the BP86 functional bracket the experimental value for Δg_{33}, whereas Δg_{22} is underestimated slightly in both calculations. The latter point is probably a basis set effect, cf. the basis set study for the free phenoxyl radical in Table 9. For the tyrosyl radical, the lower SOS-DFPT values appear to be somewhat closer to the available experimental data (we have chosen experimental numbers for tyrosyl radicals where hydrogen bonding to the phenoxyl oxygen is thought to be absent). From the present data it is difficult to decide whether the SOS-DFPT correction terms improve the results significantly for main group radicals. We have therefore concentrated on UDFT-BP86 results throughout this study. In any case, the results in Table 9 indicate that DFT approaches are significantly superior to Hartree−Fock calculations for phenoxyl radicals, comparable in quality to the (modest) MCSCF wave functions of ref 54. The advantage of DFT is the relatively low computational effort, and thus the possibility to treat large systems. Indeed, we are presently studying *g*-tensors for much larger radicals. This requires also a very efficient treatment of the spin−orbit operators, such as demonstrated in this work.

Less favorable performance of DFT was noted by PZ for *g*-tensors of transition metal complexes (a number of square pyramidal d^1 complexes were studied, see below) compared to main-group radicals.[28] This has been attributed to deficiencies of the currently used exchange-correlation functionals. Table 10 gives our results for a more diverse set of 3d complexes. In addition to the accurate atomic mean-field treatment of the $\Delta g_{SO/OZ(1e)}$ and $\Delta g_{SO/OZ(2e)}$ terms, we have also included results which neglect the $\Delta g_{SO/OZ(2e)}$ contributions altogether. Figure 2 compares the results graphically to experiment. Some care has to be exercised in this comparison, due to the varying quality and nature of the experimental data. Nevertheless, the graphical comparison indicates that, rather disappointingly, the proper inclusion of the two-electron SO terms deteriorates the agreement with experiment significantly. Neglecting the three extreme outliers (Δg_{zz} of $Cu(NO_3)_2$ and of $Cu(acac)_2$, and $\Delta g_{\perp}$ of TiF_3), we arrive at a linear fit with slope 0.59 and $R = 0.99378$. The complete neglect of the two-electron SO terms improves the slope to 1.06 ($R = 0.99381$). This is not surprising, as the two-electron terms reduce the overall *g*-shifts by ∼40−50% (cf. section 4). Neglect of the two-electron terms does in this case correspond to a scaling by a factor of ∼1.8. The three outliers mentioned are at particularly large (negative or positive) Δg values.

The slope of ∼0.59 we find upon exact treatment of the SO operators corresponds strikingly to observations made recently by Bühl et al.[57,58] when testing DFT approaches in calculations of nuclear shieldings of 3d transition metal nuclei (in particular of ^{57}Fe, but similar observations apply to ^{59}Co[59]). UDFT-GIAO calculations with GGA functionals gave slopes of ∼0.6 in comparison with experiment, with one extreme outlier (ferrocene).[57] This corresponds to a significant underestimate of the paramagnetic contributions to shielding. Bühl found that the slope could be improved to almost 1.0 by using hybrid functionals (B3LYP or B3PW91).[58] In view of the close similarity of nuclear shielding and electronic *g*-tensor, we expect that the origin of the failure of the "pure" GGA functionals in the two cases is related (most likely, the usual functionals do not describe accurately local excitations at the metal[60]). Thus, the inclusion of Hartree−Fock exchange (and of the resulting coupling terms) should improve the performance also for the *g*-tensor. In the present version of our code we cannot include Hartree−Fock exchange. However, we are presently implementing a new program which will allow this to be done. Then more accurate calculations of *g*-tensors should also become possible for transition metal compounds.[61] Until then, a simple multiplicative scaling of the SO contributions may be considered as a short-term improvement. This result contrasts somewhat with the conclusions of PZ, based on a less diverse set of complexes. PZ argued that a simple, additive constant shift (different for 3d, 4d, and 5d systems) might be used to correct the computed results.[28] We expect less problems for complexes where the spin density is largely concentrated on the ligands. In fact, GGA functionals perform excellently for nuclear shieldings of ligand atoms in transition metal systems.[9,10,11]

Finally, Table 11 compares our results and those of PZ for a number of $4d^1$ and $5d^1$ complexes. The agreement of our calculations with experiment is again not satisfactory, actually even somewhat worse than for those of PZ. This is probably due to some error compensation in the results of PZ, related to the incomplete treatment of the SO operators. The paramagnetic contributions to the nuclear shielding of 4d transition metal nuclei are known to be underestimated less dramatically by GGA functionals than in the case of 3d metals (e.g., the slope for Rh shieldings at the GIAO−BPW91 level was found to be ∼0.8[57,58]). One might thus expect 4d systems to be less critical also for *g*-tensor calculations. This is not borne out by the limited set of data given in Table 11. More calculations on a larger set of more diverse 4d complexes will be needed to settle this question.

7. Separation of *g*-Tensors into Atomic Contributions

As already mentioned, our use of a superposition of effective atomic spin−orbit operators does also offer advantages in terms of analyses of *g*-tensors. In this way we obtain a particularly straightforward separation of the $\Delta g_{SO/OZ}$ terms into atomic SO contributions. This is shown as an example for the phenoxyl radical in Table 12. We first note that the relative weights of $\Delta g_{SO/OZ(1e)}$ and $\Delta g_{SO/OZ(2e)}$ terms, as well as of SOO and SSO contributions to the latter, are essentially just as discussed above for CO^+ and H_2O^+.

The atomic analysis is performed by carrying out a number of separate calculations (which employ the same Kohn−Sham wave function and thus do not require much extra computational effort), in which atomic mean-field SO operators are only used

(56) Olsson, L.; Cremer, D. *J. Chem. Phys.* **1996**, *105*, 8995.
(57) Bühl, M.; Malkina, O. L.; Malkin, V. G. *Helv. Chim. Acta* **1996**, *79*, 742.
(58) Bühl, M. *Chem. Phys. Lett.* **1997**, *267*, 251.
(59) See, for example: Chan, C. C. J.; Au−Yeung, S. C. F.; Wilson, P. J.; Webb, G. A. *J. Mol. Struct.* **1996**, *365*, 125. Godbout, N.; Oldfield, E. *J. Am. Chem. Soc.* **1997**, *119*, 8065.
(60) Schreckenbach, G. *J. Chem. Phys.* **1999**, *110*, 11936.
(61) Alternative functionals may also be envisioned, in which exact exchange is simulated rather than treated explicitly (see, e.g.: Becke, A. D. *J. Chem. Phys.* **2000**, *112*, 4020).
(62) DeVore, C.; Weltner, W., Jr. *J. Am. Chem. Soc.* **1977**, *99*, 4700.

Table 10. Comparison of Computed and Experimental *g*-Shift Tensor Components (ppt) for a Series of 3d Transition Metal Complexes[a]

complex	component	without $\Delta g_{SO/OZ(2e)}$	with $\Delta g_{SO/OZ(2e)}$	exp.	lit (exp.)
TiF_3	$\Delta g_\perp$	−79.4	−28.3	−111.3	*b*(1)
				−121.5	*b*(2)
				−123.7	*b*(3)
$VO(L^3)_2$[c]	Δg_{zz}	−55.6	−25.7	−55.3	*c*
$VO(L^2)_2$[c]	Δg_{zz}	−48.8	−24.6	−51.3	*c*
$VO(L^1)_2$[c]	Δg_{zz}	−58.2	−28.6	−49.3	*c*
$VO(L^3)_2$[c]	Δg_{yy}	−31.5	−15.4	−23.3	*c*
$VO(L^2)_2$[c]	Δg_{yy}	−29.1	−14.5	−21.3	*c*
$VO(L^1)_2$[c]	Δg_{yy}	−24.1	−12.2	−21.3	*c*
$VO(L^3)_2$[c]	Δg_{xx}	−17.4	−8.8	−18.3	*c*
$VO(L^2)_2$[c]	Δg_{xx}	−20.2	−10.3	−19.3	*c*
$VO(L^1)_2$[c]	Δg_{xx}	−19.1	−9.7	−19.3	*c*
$Mn(CN)_5NO^{2-}$	$\Delta g_\parallel$	−1.2	−1.9	−10.1	*d*
TiF_3	$\Delta g_\parallel$	−1.8	−1.2	−11.1	*b*(1)
				−11.1	*b*(2)
				−3.7	*b*(3)
$Mn(CN)_4N^-$	$\Delta g_\parallel$	9.8	3.9	−3.3	*e*
$Mn(CO)_5$	$\Delta g_\parallel$	−1.2	−0.9	−1.7	*f*(1)
				−2.3	*f*(2)
$Fe(CO)_5^+$	$\Delta g_\parallel$	−0.6	−0.9	−1.5	*g*(1)
				−1.4	*g*(2)
ScO	$\Delta g_\perp$	−0.9	0.0	−0.5(3)	*h*(1)
				−2.8(5)	*h*(2)
ScO	$\Delta g_\parallel$	−0.2	−0.1	−0.5(3)	*h*(1)
				−0.8(7)	*h*(2)
MnO_3	$\Delta g_\parallel$	6.3	4.3	1.3	*i*
$Ni(CO)_3H$	$\Delta g_\parallel$	2.7	1.3	1.9	*j*
$Mn(CN)_4N^-$	$\Delta g_\perp$	4.7	2.1	2.2	*e*
$Co(CO)_4$	$\Delta g_\parallel$	7.1	3.3	3.6	*k*(1)
				5.0	*k*(2)
MnO_3	$\Delta g_\perp$	4.2	1.9	6.1	*i*
$Mn(CN)_5NO^{2-}$	$\Delta g_\perp$	36.3	17.9	28.8	*d*
$Mn(CO)_5$	$\Delta g_\perp$	42.6	22.6	40.7	*f*(1)
				35.7	*f*(2)
$Cu(acac)_2$	Δg_{xx}	50.1	30.6	48.7	*l*(1)
				49.6	*l*(2)
$Cu(NO_3)_2$	Δg_{xx}	45.1	28.2	49.9(5)	*m*
$Cu(NO_3)_2$	Δg_{yy}	49.3	31.0	49.9(5)	*m*
$Cu(acac)_2$	Δg_{yy}	55.4	34.7	48.7	*l*(1)
$Ni(CO)_3H$	$\Delta g_\perp$	65.0	39.8	65.1	*j*
$Fe(CO)_5^+$	$\Delta g_\perp$	89.3	48.7	81.0, 77.4	*g*(1)
				78.8, 76.6	*g*(2)
$Co(CO)_4$	$\Delta g_\perp$	137.5	79.3	127.6	*k*(1)
				126.0	*k*(2)
$Cu(NO_3)_2$	Δg_{zz}	183.0	116.3	246.6(3)	*m*
$Cu(acac)_2$	Δg_{zz}	180.2	115.5	285.2	*l*(1)
				263.8	*l*(2)

[a] UDFT-IGLO with AMFI approximation for $\Delta g_{SO/OZ(2e)}$, 9s7p4d metal basis, BIII on ligands (DZVD basis on remote atoms in $VO(L^n)_2$; BII on remote atoms in $Cu(acac)_2$). [b] Reference 62: (1) Neon, site a; (2) Neon, site b; (3) Argon. Estimated error of Δg: ±0.2 ppt. [c] The complexes are: $VO(L^1)_2$ = [*N*,*N*′-ethylenebis(*o*-*tert*-butyl-*p*-methylsalicylaldiminato)]oxovanadium(IV); $VO(L^2)_2$ = bis(*N*-methylsalicylaldiminato)oxovanadium(IV); $VO(L^3)_2$ = bis(*N*-methyl-*o*-*tert*-butyl-*p*-methylsalicylaldiminato)oxovanadium(IV). Experimental data from ref 29. Estimated error of Δg: ±1 ppt. EPR on polycrystalline substance. [d] Manoharan, T.; Gray, H. B. *Inorg. Chem.* **1966**, *5*, 823; single-crystal EPR in a host lattice of $Na_2Fe(CN)_5NO{\cdot}2H_2O$. [e] Bendix, J.; Meyer, K.; Weyhermüller, T.; Bill, E.; Metzler-Nolte, N.; Wieghart, K. *Inorg. Chem.* **1998**, *37*, 1767; EPR in frozen CH_3CN. [f] (1) Symons, M. C. R. *Organometallics* **1982**, *1*, 834; EPR in Ar matrix. Estimated error of Δg: ±10 ppt. (2) EPR in C_6D_6 matrix: Howard, J. A.; Morton, J. R.; Preston, K. F. *Chem. Phys. Lett.* **1982**, *83*, 1226. Estimated error of Δg: ±3 ppt. [g] EPR in $Cr(CO)_6$ host crystal, Lionel, T.; Morton, J. R.; Preston, K. F. *J. Chem. Phys.* **1982**, *76*, 234. (1) site a, (2) site b. For the perpendicular components, experimental Δg_{xx}, Δg_{yy} are given. [h] Knight, L. B.; Kaup, J. G.; Petzoldt, B.; Ayyad, R.; Ghanty, T. K.; Davidson, E. R. *J. Chem. Phys.* **1999**, *110*, 5658; (1) EPR in Ne matrix, (2) EPR in Ar matrix. [i] Ferrante, F.; Wilkerson, J. L.; Graham, W. R. M.; Weltner, W., Jr. *J. Chem. Phys.* **1977**, *67*, 5906. EPR in Ne matrix. Estimated error of *g*: ±0.8 ppt. [j] Morton, J. R.; Preston, K. F. *J. Chem. Phys.* **1984**, *81*, 5775. EPR in Kr matrix. Estimated error of *g*: ±0.2 ppt. [k] (1) EPR in solid Kr; Fairhust, S. A.; Morton, J. R.; Preston, K. F. *J. Magn. Reson.* **1983**, *55*, 453.; (2) EPR in CO matrix, Hanlan, L. A., Huber, H.; Kündig, E. P.; McGarvey, B. R.; Ozin, G. A. *J. Am. Chem. Soc.* **1975**, *97*, 7054. Estimated error of Δg: ±10 ppt. [l] (1) Wilson, R.; Kivelson, D. *J. Chem. Phys.* **1966**, *44*, 4445. Radicals trapped in chloroform glass. (2) Maki, A. H.; McGarvey, B. R. *J. Chem. Phys.* **1958**, *29*, 31, 35. EPR in host crystal of $Pd[(CH_3CO)_2CH]_2$. [m] Kasai, P. H.; Whipple, E. B.; Weltner, W., Jr. *J. Chem. Phys.* **1966**, *44*, 2581. EPR in Ne matrix.

on specific atoms or sets of atoms. The sums of these contributions do in all cases studied correspond closely to the overall $\Delta g_{SO/OZ}$ results, as they should. The analysis for the phenoxyl radical shows, as expected in this case,[54] that SO coupling at the oxygen atom dominates the Δg_{22} and Δg_{33} components. The other atomic contributions are much smaller but not always negligible. Thus, for example, contributions from SO coupling at the ortho carbon atoms reduce Δg_{33} but enhance Δg_{22}. We may go one step further and decompose also individual molecular orbital contributions into their atomic SO constituents. Table 12 shows this as an example for the in-plane π b_1 HOMO. The coupling of the β-part of this MO (cf. Figure 3a) with the unoccupied β -part of the out-of-plane π b_2 SOMO (Figure 3b) is known[54] to dominate Δg_{33} (contributions from several occupied MOs with σ(C−O) bonding character dominate Δg_{22}). This is confirmed by the entry in Table 12. The further

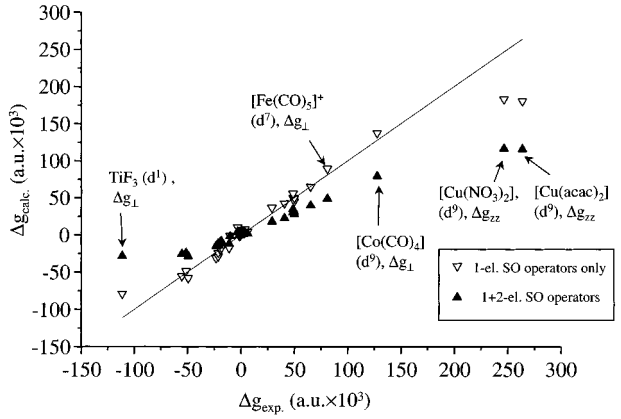

Figure 2. Comparison of calculated and experimental *g*-shift tensor components (ppt) for 3d transition metal complexes (cf. Table 10).

Table 11. *g*-Shift Tensor Results (ppt) for Some Square Pyramidal $4d^1$ and $5d^1$ Complexes

	ECP−SO[a]		PZ[b]		exp.[c]	
	$\Delta g_{\|\|}$	$\Delta g_{\perp}$	$\Delta g_{\|\|}$	$\Delta g_{\perp}$	$\Delta g_{\|\|}$	$\Delta g_{\perp}$
$MoOF_4^-$	−59	−51	−62	−57	−107	−76
$MoOCl_4^-$	+12	−38	+6	−43	−37	−55
$MoOBr_4^-$	+119	−29	+142	−31		
$MoNCl_4^{2-}$	−35	−6	−47	−9	−96	−18
$WOCl_4^-$	−31	−120	−68	−139		
$TcNF_4^-$	−43	−15	−41	−16	−107	−12
$TcNCl_4^-$	+47	+8	+43	+6	+6	−2
$TcNBr_4^-$	+187	+64	+212	+75	+145	+32
$ReOF_4$	−123	−156	−132	−177		
$ReOCl_4$	+106	−117	+80	−141	−28	−294
$ReOBr_4$	+253	−84	+257	−117	+168	−237
$ReNF_4^-$	−189	−57	−187	−70	−353	
$ReNCl_4^-$	+46	−7	+9	−17	−88	−57
$ReNBr_4^-$	+185	+40	+174	+33	+67	−29

[a] This work, UDFT-IGLO, BP86. Quasirelativistic ECP/SO-ECP calculations. [b] UDFT-GIAO, BP86, ref. 28. [c] Experimental data as compiled in ref 28.

atomic decomposition of the HOMO contribution shows again clearly the dominance of oxygen SO coupling, but also the negative contributions from the ortho carbon atoms, which reduce the Δg_{33} component.

While the dominance of oxygen SO coupling has been obvious in the previous example, Table 13 shows two examples, $CrOF_4^-$ and $CrOCl_4^-$, in which several atoms contribute nonnegligibly. We may first examine the atomic break-down of the total *g*-shift components. In both cases, SO coupling from the metal dominates the negative $\Delta g_{\perp}$. In contrast, halogen SO coupling contributes positively to $\Delta g_{\|}$. While the negative metal contribution is larger and dominates in $CrOF_4^-$, the halogen contribution in $CrOCl_4^-$ dominates, and a relatively small, positive $\Delta g_{\|}$ results (experimentally, this component is also small but negative, cf. Table 6).

MO analyses of the *g*-tensors for these types of C_{4v}-symmetrical d^1 complexes have already been discussed in detail,[28] and we refer the reader to that work for the MO notation. In Table 13, we go a step further and decompose the most important MO contributions into their atomic constituents. The above-mentioned compensation between metal and halogen SO coupling for $\Delta g_{\|}$ arises in an interesting manner. Metal SO coupling contributes negatively via the SOMO but positively via the b_1 MO, and in the case of $CrOCl_4^-$ also via the e MOs. Halogen SO coupling contributes positively through all three MOs. In contrast, metal SO coupling dominates $\Delta g_{\perp}$ mainly via the negative SOMO contribution. These results are just

Table 12. Break-Down of *g*-Shift Tensor (ppm) for the Phenoxyl Radical[a]

	Δg_{11}	Δg_{22}	Δg_{33}
$\Delta g_{GC(1e)}$	188	268	186
Δg_{RMC}	−198	−198	−198
$\Delta g_{SO/OZ(1e)}$	−95	3574	13110
$\Delta g_{SO/OZ(2e)}$ (SSO[b], SOO[c])	97 (97[b], 0[c])	−1410 (−1087[b], −323[c])	−4729 (−3638[b], −1091[c])
total	−8	2234	8369
break-down into atomic contributions[d]			
O	3	1734	8685
C_{ipso}	0	48	−4
C_{ortho}(2x)	0	283	−358
C_{meta}(2x)	4	−42	−92
C_{para}	−3	141	150
H (5x)	0	0	0
Σ	2	2164	8381
total $\Delta g_{SO/OZ}$	2	2164	8381
HOMO contribution	40	−8	7748
atomic break-down of the HOMO contribution[d]			
O	41	−1	8178
C_{ipso}	0	−1	123
C_{ortho}(2x)	4	−5	−620
C_{meta}(2x)	−5	−5	−24
C_{para}	0	−1	94
H (5×)	0	−1	1
Σ	40	−14	7752

[a] UDFT-BP86 calculations with common gauge at center of mass, BIII basis, and AMFI approximation. [b] Spin−same-orbit contribution. [c] Spin−other-orbit contribution. [d] Atomic mean-field SO operators were employed only on the specified atoms in each case (see text).

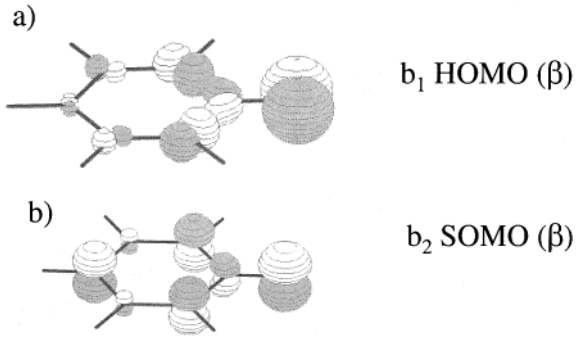

Figure 3. Display of Kohn−Sham orbitals for the phenoxyl radical as isosurface (±0.1 au). (a) *β*-component of HOMO (b_1). (b) *β*-component of SOMO (b_2).

illustrative examples of the additional insight that is provided by the use of SO operators which are accurate and yet atomic in nature. Analyses of this type should become useful for a large variety of questions related to the interpretation of electronic *g*-tensors.

8. Conclusions

We have implemented and validated DFT calculations of the electronic *g*-tensor of EPR spectroscopy including all the relevant perturbation operators and IGLO gauge origins. The main advantage of the present approach lies in the treatment of spin−orbit coupling. To our knowledge, both the all-electron atomic mean-field approximation to the complete Breit−Pauli SO operators and the combination of quasirelativistic ECPs with SO-ECPs have been used here for the first time in *g*-tensor calculations. Both approximations provide an inexpensive but accurate way to include SO coupling. Agreement of the mean-field SO treatment with the full-blown explicit treatment of all

Table 13. Break-Down of *g*-Shift Tensor (ppt) for $CrOX_4^-$ (X = F, Cl)[a]

	$CrOF_4^-$		$CrOCl_4^-$	
	$\Delta g_{\|\|}$	$\Delta g_\perp$	$\Delta g_{\|\|}$	$\Delta g_\perp$
break-down into atomic contributions[b]				
Cr	−25	−21	−11	−18
X	10	0	30	1
O	0	−1	0	−1
Σ	−15	−22	19	−18
total $\Delta g_{SO/OZ}$	−15	−22	19	−18
atomic break-down of dominant MO contributions[c]				
SOMO (b_2, "d_{xy}")				
Cr	−34	−20	−28	−16
X	7	−1	19	0
O	0	0	0	0
Σ	−27	−21	−9	−16
σ-MO (b_1)				
Cr	12	0	10	1
X	5	0	5	3
O	0	0	0	0
Σ	17	0	15	4
π(Cr−O) MOs (e)				
Cr	−3	0	6	−2
X	0	0	10	−2
O	0	0	0	0
Σ	−3	0	16	−4

[a] UDFT-BP86 results with BII basis, AMFI approximation, and common gauge at the center of mass. Cf. Table 6 for the IGLO results (and for a decomposition into first- and second-order terms). [b] Atomic mean-field SO operators were employed only on the specified atoms in each case (see text). [c] Cf. ref 28 for a more detailed discussion of the MO contributions.

one- and two-electron SO integrals is essentially quantitative at a small fraction of the computational cost of the latter, as found previously in other applications of this approach. In turn, SO-ECPs approximate well the mean-field all-electron approach, with the additional advantage of a very efficient simultaneous inclusion of scalar relativistic effects. The pseudopotential approximation is particularly fruitful for a property like the *g*-tensor, which is to a large extent a property of the valence electrons. Due to the atomic nature of both all-electron mean-field operators and SO-ECPs, the two approaches may furthermore be combined in one calculation. In addition to a significant improvement in computational efficiency, this fact simplifies the analysis of *g*-tensors by allowing a separation into atomic SO contributions.

Having been able to include SO coupling accurately for larger systems, we could evaluate the performance of DFT approaches for the calculation of *g*-tensors without significant errors to be expected from approximate SO operators. We find that gradient-corrected exchange-correlation functionals perform very well for main-group species. This opens the way to quantitative calculations of *g*-tensors in a wide variety of applications, for example, for phenoxyl or semiquinone radicals or for other spin labels in biological systems. Larger discrepancies found for some compounds of heavier atoms (e.g., for the anions CF_3X^-, see Table 4) may partly be due to the neglect of environmental effects.

In contrast to the good performance for main-group species, the results obtained for transition metal complexes are much less satisfactory. We agree with Patchkowski and Ziegler[28] in attributing this less favorable performance for transition metal systems to deficiencies in the gradient-corrected functionals. The present results for a rather diverse set of 3d transition metal complexes indicate that the paramagnetic ($\Delta g_{SO/OZ}$) contributions are underestimated systematically. A simple multiplicative scaling of these terms improves the overall agreement with experiment but is certainly not satisfactory from a theoretical point of view. We have also pointed out that similar problems have been observed by Bühl et al. for NMR chemical shifts of transition-metal nuclei.[57,58] In the latter case, the use of exchange-correlation functionals that include some exact, non-local exchange, enabled much more accurate calculations. We expect this to be the case also for *g*-tensor calculations on systems in which the spin density is mainly localized on a transition metal. We are thus presently implementing a code which will allow such hybrid functionals to be used also for the calculation of *g*-tensors.

A further potential source of errors stems from the first-order perturbation theoretical treatment of SO coupling. This may affect the results for systems with very heavy atoms. Therefore, our ongoing work involves also a two-component relativistic approach that covers SO coupling variationally. Despite the obvious need for further methodological improvements, the present approach should provide a very powerful tool to study electronic *g*-tensors in a large variety of areas ranging from materials research to biochemistry.

Acknowledgment. We thank Drs. H. Stoll (Stuttgart), H.-J. Flad (Leipzig), and P. Pyykkö (Helsinki) for helpful discussions. V.G.M. and O.L.M. gratefully acknowledge financial support from the Slovak Grant Agency VEGA (Grant No. 2/7203/00) and from the COST chemistry program (Project D9/0002/97), and they thank the Computing Center of the Slovak Academy of Sciences for computational resources. J.V. is on leave from the University of Oulu, Department of Physical Sciences, Oulu, Finland, and has been supported by the Marie Curie program (Contract No. ERBFMBICT982911) of the European Commission. Further support has been provided within the Graduiertenkolleg "Moderne Methoden der magnetischen Resonanz" in Stuttgart (scholarship to B.S. and travel costs), by Deutsche Forschungsgemeinschaft (Heisenberg scholarship to M.K. and Schwerpunktprogramm "Relativistische Effekte in der Chemie und Physik schwerer Elemente"), and by the Fonds der Chemischen Industrie.

Supporting Information Available: Tables S1−S5 give optimized Cartesian coordinates for the phenoxyl, 2,4,6-tris-*t*-Bu-C_6H_2O and tyrosyl radicals, as well as for $Cu(acac)_2$ and $Cu(NO_3)_2$ (PDF). This material is available free of charge via the Internet at http:pubs.acs.org.

JA000984S